WOLFF, P. M. DE (1974). *Acta Cryst.* A30, 777-785.
WOLFF, P. M. DE (1977). *Acta Cryst.* A33, 493-497.
WOLFF, P. M. DE, JANSSEN, T. & JANNER, A. (1981). *Acta Cryst.* A37, 625-636.
YAMAMOTO, A. (1980). *Phys. Rev. B*, **22**, 373-379.
YAMAMOTO, A. (1982*a*). *REMOS*.82. A computer program for refinement of modulated structures. National Institute for Research in Inorganic Materials, Sakura-mura, Niihari-gun, Ibaraki 305, Japan.
YAMAMOTO, A. (1982*b*). *Acta Cryst.* A38, 87-92.

Acta Cryst. (1987). B43, 368-376

LEED Intensity Analysis of the Structure of Coadsorbed Benzene and CO on Rh(111)

BY R. F. LIN,* G. S. BLACKMAN, M. A. VAN HOVE† AND G. A. SOMORJAI

Materials and Molecular Research Division, Lawrence Berkeley Laboratory, and Department of Chemistry, University of California at Berkeley, Berkeley, California 94720, *USA*

(*Received* 27 *October* 1986; *accepted* 24 *March* 1987)

Abstract

The structure of benzene coadsorbed with CO on Rh(111) has been analyzed using low-energy electron diffraction (LEED) interpreted by dynamical calculations. The present structure, Rh(111)-(3×3)-C_6H_6+2CO, complements an earlier result for the system Rh(111)-$\binom{31}{13}$-C_6H_6+CO, but is distinguished by a different ratio of benzene to CO molecules. The main characteristics of the molecule–metal bonding are substantially confirmed: intact benzene lying flat and centered over h.c.p.-type hollow sites with an expanded C_6 ring, and CO standing upright on the same type of hollow site. These two structures are also compared and contrasted with a recent analysis of the structure of benzene coadsorbed with CO on Pt(111), for which bridge sites occur and a larger C_6 ring expansion is found.

1. Introduction

As part of an ongoing study of the structural chemistry of hydrocarbons on transition metal surfaces, we report two structures of benzene adsorbed on the Rh(111) single-crystal surface in the presence of coadsorbed carbon monoxide. The first structure, Rh(111)-$\binom{31}{13}$-C_6H_6+CO, has already been published (Van Hove, Lin & Somorjai, 1983, 1986) and is recalled here for comparison [the $\binom{31}{13}$ matrix notation is equivalent to the $c(2\sqrt{3}\times4)$rect notation, also used in these references]. The second structure, Rh(111)-(3×3)-C_6H_6+2CO, is new and substantially confirms important aspects of the first structure.

Many techniques have been used to study benzene on transition metal surfaces (Nyberg & Richardson, 1979; Tsai & Muetterties, 1982; Massardier, Tardy, Abon & Bertolini, 1983; Surman, Bare, Hofmann & King, 1983; Koel, Crowell, Mate & Somorjai, 1984; Neumann, Mack, Bertel & Netzer, 1985). Our work is based primarily on low-energy electron diffraction (LEED) and high-resolution electron-energy-loss spectroscopy (HREELS). As was observed by thermal desorption spectroscopy (TDS) and HREELS (Mate & Somorjai, 1985), the (3×3) benzene structure on Rh(111) differs from the $\binom{31}{13}$ structure in the molecular ratio C_6H_6:CO, namely 1:2 *vs.* 1:1, respectively.

There also exists a CO-free ordered benzene structure on Rh(111), with a $(2\sqrt{3}\times3)$ rect $=\binom{44}{22}$ superlattice (Mate & Somorjai, 1985). Although this structure has not been analyzed in detail, its principal features are known and provide an interesting comparison with the CO coadsorbate systems. Furthermore, a parallel sequence of benzene/CO structures exists on Pt(111) (Gland & Somorjai, 1973; Mate & Somorjai, 1985), one of which has been structurally analyzed in detail (Ogletree, Van Hove & Somorjai, 1987). The interaction between the coadsorbates can manifest itself both in ordering and in bonding effects: the long-range order depends on the relative coverage of the two coadsorbed molecules, and each molecule bonds very differently to the metal in the absence of the other molecule.

2. LEED analysis of the (3×3) structure

2.1. *LEED experiment*

The Rh(111) single-crystal surface was cleaned by repeated cycles of heating in oxygen, argon sputtering and annealing (Lin, Koestner, Van Hove & Somorjai, 1983). Cleanliness was verified by Auger electron spectroscopy. The data used for this surface structure analysis were obtained at normal incidence. The crystal was oriented to within ~0·2° of normal incidence

* Permanent address: Department of Physics, Fudan University, Shanghai, People's Republic of China.
† Direct inquiries about computational details to this author.

0108-7681/87/040368-09$01.50

by slowly varying the θ angle and observing symmetry-equivalent beams.

The Rh(111)–(3×3) pattern was obtained by first dosing the crystal with approximately $\frac{2}{9}$ monolayer of CO [to provide two CO molecules per (3×3) unit cell]; then saturating the surface with benzene. This produced a single complete molecular layer on the metal substrate. Calibration of the CO coverage was possible by comparison with the solved Rh(111)–$(\sqrt{3}\times\sqrt{3})R30°$–CO structure, which corresponds to $\frac{1}{3}$ monolayer of CO. CO gas of 99·98% purity was used with no further purification. The benzene was dried over a desiccant and degassed using several cycles of freezing with liquid nitrogen followed by pumping with a sorption pump.

LEED intensities were obtained as a function of electron kinetic energy from a standard 4 grid LEED optics by both the photographic method (Lin, Koestner, Van Hove & Somorjai, 1983) and the video-camera method (Ogletree, Katz & Somorjai, 1986) with excellent reproducibility. Because of the possibility of electron beam damage in these organic overlayers, sequential data sets were taken under identical conditions. Subsequent analysis of absolute peak intensities indicated an insignificant amount of beam damage. In our LEED intensity analysis, we have used intensity–energy (I–V) curves for 14 symmetry-inequivalent beams measured at normal incidence, with an energy range of 20–200 eV. These beams are labeled (0, −1), (1, −1), (1, −2), (0, $-\frac{2}{3}$), ($\frac{2}{3}$, $-\frac{2}{3}$), ($\frac{1}{3}$, $-\frac{2}{3}$), ($\frac{1}{3}$, −1), ($\frac{2}{3}$, −1), ($\frac{2}{3}$, $-\frac{4}{3}$), (1, $-\frac{4}{3}$), (0, $-\frac{4}{3}$), ($\frac{4}{3}$, $-\frac{4}{3}$), ($\frac{4}{3}$, $-\frac{1}{3}$), (0, $-\frac{5}{3}$). The LEED pattern and beam labeling are illustrated in Fig. 1, together with a real-space representation of the unit cell. The cumulative energy range (added over the 14 beams) was 1144 eV.

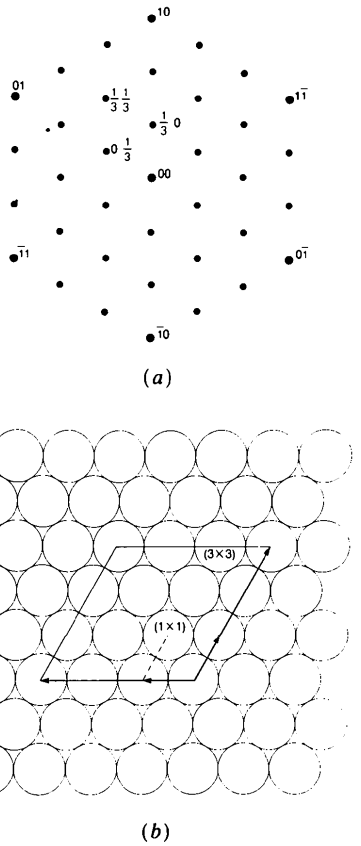

Fig. 1. Schematic LEED pattern with beam labeling (*a*) and corresponding surface unit cell for a (3×3) overlayer on Rh(111) (*b*).

2.2. *LEED theory*

The theory underlying the LEED calculations used to interpret the experimental data has been described elsewhere (Van Hove, Lin & Somorjai, 1986). We give here a summary of the various calculational techniques applied in this work. Our basis is a multiple-scattering theory, called the combined space method and extended to include a number of approximations. The structural search was conducted in steps of increasing theoretical accuracy, as the search narrowed down the list of plausible structures. For the molecular overlayer we started with the kinematic approximation to obtain layer diffraction matrices. Better accuracy was obtained with a near-neighbor multiple-scattering version of reverse scattering perturbation (RSP), in which multiple-scattering paths were allowed to connect only near-neighbor atoms within the overlayer. Also, a full version of RSP was employed, allowing all multiple scattering to full convergence within the overlayer. Finally, the highest accuracy was obtained with matrix inversion rather than RSP. In all these cases, the substrate and the stacking of the overlayers onto the substrate were treated with full multiple scattering (within the renormalized forward scattering scheme), before inclusion of coadsorbed CO in addition to benzene. To compensate efficiently for the added computational effort due to coadsorption, we applied beam set neglect (BSN), a powerful approximation to handle large unit cells. Another efficient technique, kinematic sublayer addition (KSLA), was chosen to handle the coadsorbates, for which individual scattering properties (with any amount of internal multiple scattering included) are added kinematically into a set of overlayer diffraction matrices. The exact sequence of calculational techniques used will be shown in Table 1. The final most accurate calculations are believed to provide a structural accuracy of better than 0·1 Å (this value varies somewhat with the structural parameter), based on a variety of tests carried out during this work and previously.

The nonstructural parameters of the calculations (electron mean-free path, Debye temperature, atomic scattering phase shifts *etc.*) were the same as those used in our earlier work (Van Hove, Lin & Somorjai, 1986; Ogletree, Van Hove & Somorjai, 1986). The number of phase shifts used ($l_{max}+1$) was 5 during

Table 1. *Structures tested by LEED intensity calculations*

Composition	Site[a]	φ(°)[b]	$d_{\perp M-C_6}$ (Å)[c]	Buckling[d]	d_{C-C} (Å)[e]	Method[f]
C_6H_6	*aABC, bABC, cABC*	0, 15, 30	1·2 (0·3) 3·9	None	1·397	Kinematic
C_6H_6	*aABC*	0, 30	1·5 (0·1) 1·9	None	1·397	Partial & full RSP
C_6H_6	*bABC*	0, 30	2·9 (0·1) 3·3	None	1·397	Partial & full RSP
C_6H_6	*cABC*	0, 30	1·9 (0·1) 2·3	None	1·397	Partial & full RSP
C_6H_6	*aABC*	Spinning[g]	1·5 (0·1) 1·9	None	1·397	Kinematic
C_6H_6	*bABC*	Spinning	2·9 (0·1) 3·3	None	1·397	Kinematic
C_6H_6	*cABC*	Spinning	1·9 (0·1) 2·3	None	1·397	Kinematic
C_6H_6	*dABC*	0, 30 Spinning	1·2 (0·2) 4·0	None	1·397	Kinematic
C_6H_6	*aABC, bABC, cABC*	0	1·2 (0·3) 3·9	None	1·54	Kinematic
C_6H_6	*aABC, bABC, cABC*	0	1·2 (0·3) 3·9	None	(1·33, 1·54)[h]	Kinematic
C_6H_6	*dABC*	0, 30	1·2 (0·2) 4·0	None	1·54	Kinematic
C_6H_6	*dABC*	0	1·2 (0·2) 4·0	None	(1·33, 1·54)[h]	Kinematic
C_6H_6	*dABC*	0	1·2 (0·2) 4·0	None	(1·54, 1·33)[h]	Kinematic
C_6H_6	*aABC, bABC, cABC*	±30	1·2 (0·3) 3·9	Chair[i]	1·54	Kinematic
C_6H_6	*dABC*	0	1·2 (0·2) 4·0	Boat up[j] 0·3, 0·5 Å	1·54	Kinematic
C_6H_6	*dABC*	0	1·2 (0·2) 4·0	Boat down[j] 0·3, 0·5 Å	1·54	Kinematic
C_6H_6	*aABC, bABC, cABC*	0, 30	1·6 (0·1) 2·5	None	[1·33, 1·64 (0·43) 3·36][h]	Kinematic
C_6H_6	*bABC, cABC*	0	1·65 (0·15) 2·25	None	1·397	Kinematic

Composition	Site[a] C_6H_6	Site[a] C	φ(°)[b]	$d_{\perp C-C_6}$ (Å)[l]	d_{C-C} (Å)[e]	$d_{\perp M-C_1}$ (Å)[k]	Method[f]
C_6H_6+C	*bABC*	*bABC*[m]	0	0·55 (0·15) 1·15	1·397	1·10 (0·15) 1·70	BSN + partial RSP
C_6H_6+C	*cABC*	*cABC*[m]	0	0·55 (0·15) 1·15	1·397	1·10 (0·15) 1·70	BSN + partial RSP
C_6H_6+C	*bABC*	*bABC*[m]	0	0·40 (0·2) 1·60	1·397	1·10 (0·20) 1·50	BSN + full RSP
C_6H_6+C	*cABC*	*cABC*[m]	0	0·40 (0·2) 1·60	1·397	1·10 (0·20) 1·50	BSN + full RSP
C_6H_6+2C[n]	*bABC*	2×*bABC*	0	0·55 (0·15) 1·15	1·397	1·10 (0·15) 1·70	BSN + partial RSP
C_6H_6+2C[n]	*cABC*	2×*cABC*	0	0·55 (0·15) 1·15	1·397	1·10 (0·15) 1·70	BSN + partial RSP
C_6H_6+2C[o]	*bABC*	*bABC*[m]	0	0·55 (0·15) 1·15	1·397	1·10 (0·15) 1·70	BSN + partial RSP
C_6H_6+2C[o]	*cABC*	*cABC*[m]	0	0·55 (0·15) 1·15	1·397	1·10 (0·15) 1·70	BSN + partial RSP

Composition	Site[a] C_6H_6	Site[a] CO	φ(°)[b]	$d_{\perp C-C_6}$(Å)[s]	Ring distortion[p] r (Å)	Ring distortion[p] β(°)	$d_{\perp M-CO}$ (Å)[r]	d_{C-O} (Å)[q]	Method[f]
C_6H_6+2CO	*aABC*	2×*aABC*	0	−0·2 (−0·2) −0·8	1·397	0	1·3 (0·1) 2·4	1·15	BSN + KSLA + RSP
C_6H_6+2CO	*bABC*	2×*bABC*	0	0·55 (0·2) 1·15	1·397	0	1·3 (0·1) 2·4	1·15	BSN + KSLA + RSP
C_6H_6+2CO	*cABC*	2×*cABC*	0	0·55 (0·2) 1·15	1·397	0	1·3 (0·1) 2·4	1·15	BSN + KSLA + RSP
C_6H_6+2CO	*dABC*	2×*dABC*	0, 30	0·25 (0·2) 0·85	1·397	0	1·3 (0·1) 1·8	1·15	BSN + KSLA + RSP
C_6H_6+2CO	*bABC*	2×*bABC*	0	0·5 (0·2) 1·1	1·2 (0·17) 1·71	−5·0 (2·5) 7·5	1·25 (0·05) 1·50	1·15	BSN + KSLA + MINV (6 phase shifts)
C_6H_6+2CO	*bABC*	2×*bABC*	0	0·5 (0·2) 1·1	1·397	0	1·25 (0·05) 1·50	1·15	BSN + KSLA + MINV (6 phase shifts)
C_6H_6+2CO	*dABC*	2×*dABC*	0	0·5 (0·2) 1·1	1·397	0	1·3 (0·1) 1·8	1·15	BSN + KSLA + MINV (6 phase shifts)
C_6H_6+2CO	*bABC*	2×*bABC*	0	0·9	1·2 (0·17) 1·71	±3·75, 7·5	1·15 (0·05) 1·4	1·15	BSN + KSLA + MINV (6 phase shifts)
C_6H_6+2CO	*bABC*	2×*bABC*	0	0·5 (0·2) 1·1	1·51	−1·3	1·15 (0·05) 1·4	1·15 (0·05) 1·25	BSN + KSLA + MINV (6 phase shifts)

Notes:

(*a*) *aABC* = adsorbate centered on top site, *bABC* = on h.c.p. hollow site, *cABC* = on f.c.c. hollow site, *dABC* = on bridge site.

(*b*) Azimuthal orientation of C_6 ring (see Figs. 2*a,b*).

(*c*) Smallest layer spacing between metal-atom nuclei and C_6 nuclei; notation $d_1(\Delta d)d_2$ implies values from d_1 to d_2 in steps of Δd.

(*d*) Out-of-plane distortion of C_6 ring, if any.

(*e*) C–C bond length(s) in C_6 ring.

(*f*) Calculational method (5 phase shifts used, unless otherwise noted); kinematic = all kinematic in overlayer; partial RSP refers to near-neighbor multiple scattering only; RSP = reverse scattering perturbation; BSN = beam set neglect; KSLA = kinematic sublayer addition; MINV = matrix inversion instead of RSP.

(*g*) 'Spinning' C_6H_6 molecules are achieved by averaging among overlayers with different values of φ between 0 and 60°.

(*h*) Kekulé distortion with alternating short and long C–C bonds.

(*i*) Cyclohexane C_6 structure in chair arrangement, using tetrahedral C–C–C angles.

(*j*) Cyclohexane C_6 structure in boat arrangement, with tips tilted up or down with respect to C_6 median plane (// surface plane) by 0·3 or 0·5 Å.

(*k*) Smallest layer spacing between metal-atom nuclei and carbon nuclei of coadsorbate.

(*l*) Smallest layer spacing between single-carbon nuclei and C_6 nuclei.

(*m*) Two *bABC* and *cABC* sites are available for C, inequivalent with respect to the C_6H_6 orientation: both were tried.

(*n*) Two individual C atoms per unit cell.

(*o*) One pair of C atoms, one above the other a distance $d_{\perp C-C}$ = 1·15 and 1·45 Å, similar to ethylidyne.

(*p*) Kekulé distortions only, characterized by r and β (see Fig. 2*d*).

(*q*) C–O bond length (C–O bond always perpendicular to surface).

(*r*) Smallest layer spacing between metal-atom nuclei and C nuclei of CO.

(*s*) Smallest layer spacing between C nuclei of CO and C_6 nuclei.

most of the structural search and 6 in the final stages. Hydrogen was ignored, as usual.

We have applied R factors to evaluate the level of agreement between theoretical intensities I_t and experimental intensities I_e for the various structural models. We have used the following five R factors together with their average

ROS = fraction of energy range with slopes of opposite signs in the experimental and theoretical I-V curves

$$R1 = 0{\cdot}75 \int |I_e - cI_t| \mathrm{d}E / \int |I_e| \mathrm{d}E,$$

$$R2 = 0{\cdot}5 \int (I_e - cI_t)^2 \mathrm{dE} / \int I_e^2 \mathrm{d}E,$$

$$R\mathrm{RZJ} = 0{\cdot}5 \int \{|I_e'' - cI_t''\|I_e' - cIt_t'| \times (|I_e'| + \max|I_e'|)^{-1}\} \mathrm{d}E \times (0{\cdot}027 \int |I_e| \mathrm{d}E)^{-1},$$

$$R\mathrm{PE} = 0{\cdot}5 \int (Y_e - Y_t)^2 \mathrm{d}E / \int (Y_e^2 + Y_t^2) \mathrm{d}E,$$

$$Y(E) = L/(1 + V_{oi}^2 L^2), \; L = I'/I.$$

Here $c = \int |I_e| \mathrm{d}E / \int |I_t| \mathrm{d}E$ and the prime denotes differentiation with respect to energy. RRZJ is the reduced Zanazzi-Jona R factor, while RPE is Pendry's R factor, both renormalized with a factor 0·5 to match the scale of the other R factors (V_{oi} is an estimate of the imaginary part of the inner potential, here 4 eV). We shall mainly use the average over these five R factors, but we shall also quote $2 \times R$RZJ and $2 \times R$PE to allow comparison with other work. These R factors have been used in many previous surface structure studies with LEED (Van Hove, Lin & Somorjai, 1983, 1986; Ogletree, Van Hove & Somorjai, 1986).

2.3. (3×3) *Structures tested*

In many ways, the structural search for the (3×3) structure paralleled that for the $\binom{31}{13}$ structure (Van Hove, Lin & Somorjai, 1986). Based on the unit-cell size, the TDS data and the HREELS data, as well as the approximate van der Waals sizes of benzene and CO, the benzene molecules were assumed to lie parallel to the Rh(111) surface, while the CO molecules were taken to stand perpendicular to the surface. High-symmetry sites were assumed, see Table 1 and Fig. 2. Since a free azimuthal rotation of benzene about the surface normal (φ rotation) could not be excluded, that possibility was considered, called 'spinning' structure in Table 1. Out-of-plane distortions (bucklings) of the C_6 ring were also considered, with shapes related to that of cyclohexane (C_6H_{12}) in chair and boat forms. Because the role of CO was at first not clear, we started with CO-free structures. This left vacancies between the benzene molecules, all or some of which were later filled with individual C atoms or ethylidyne ($\equiv$C–CH$_3$). Table 1 gives the chronological sequence of structures tested.

Then, new TDS and HREELS experiments (Mate & Somorjai, 1985) indicated the presence of about two CO molecules per benzene molecule, the CO molecules probably being in hollow sites. Thus, both vacancies in the benzene layer were filled with CO molecules. The azimuthal orientation of benzene is then most likely constrained by steric hindrance to a value of $\varphi = 0°$, as exhibited in Figs 2(*a*) and (*b*).

In-plane Kekulé-type distortions were extensively investigated. These consist of alternating long and

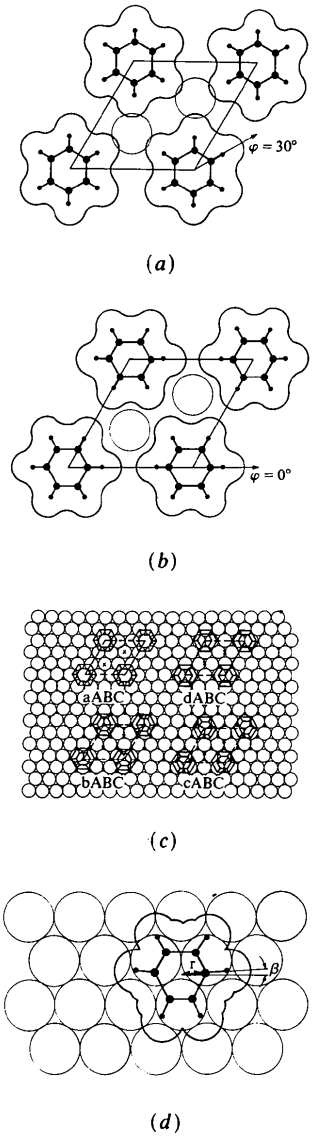

Fig. 2. (*a*) and (*b*) The molecular packing within the (3×3) overlayer on Rh(111) with van der Waals contours, for two benzene orientations ($\varphi = 0$ and 30°) and two CO molecules per unit cell. (*c*) Four 'registries' of the (3×3) overlayer (with $\varphi = 0°$) with respect to the substrate. The benzenes are represented by rings of C and H atoms, the CO by crosses. Note atoms in the second metal layer, represented by dots, and distinguishing registries *bABC* and *cABC*. The Kekulé distortion of benzene is defined in (*d*).

short C–C bonds within the C_6 rings with C_{3v} symmetry. Two variables can be used to describe a Kekulé distortion (see Fig. 2*d*): a radius r and an angular departure β from sixfold symmetrical positions. Note that in the benzene adsorption sites preferred by the LEED analysis (the hollow sites) and with $\varphi = 0°$ the Kekulé distortion has the same symmetry as the site itself. Furthermore, no out-of-plane buckling of the C_6 ring respects the site symmetry when $\varphi = 0°$. Altogether, over 1600 distinct structural geometries were tested.

Representative R factor contour plots are shown in Fig. 3. They illustrate the sensitivity to various structural parameters.

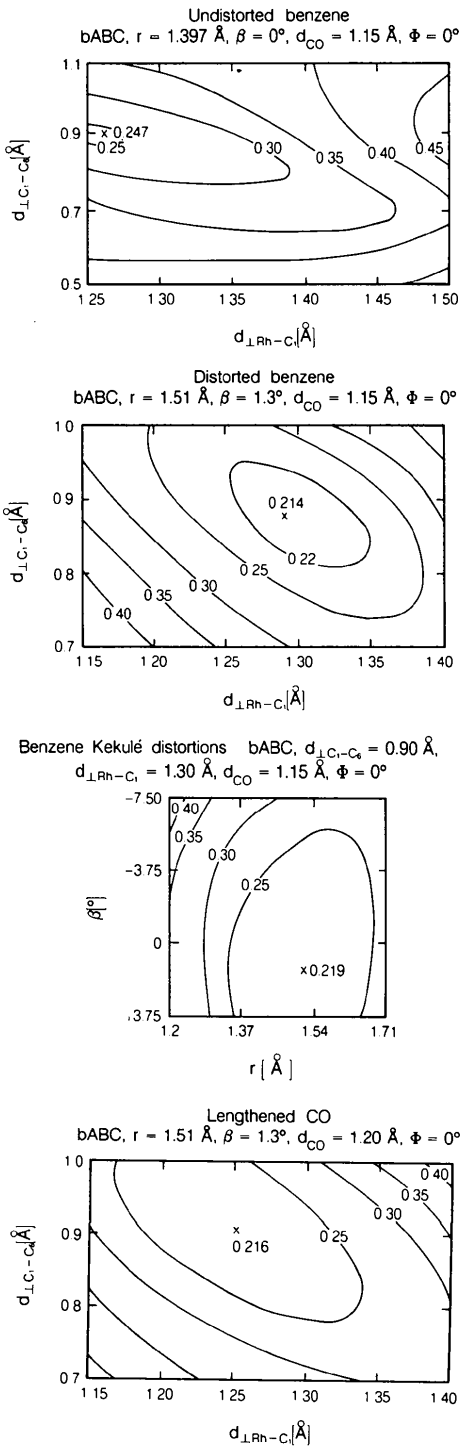

Fig. 3. R-factor contour plots for pairs of structural variables; related are the CO and C_6H_6 heights over the metal surface ($d_{\perp Rh\text{-}C_1}$, and $d_{\perp C_1\text{-}C_6}$, respectively), benzene Kekulé distortions (given by r and β, see Fig. 2*d*) and the C–O bond length.

3. Results

Minimization of the R factors yields our best structure for Rh(111)-(3×3)-C_6H_6+2CO, illustrated in Fig. 4.

In the (3×3) structure, both benzene and CO are centered on h.c.p.-type hollow sites in a compact arrangement, as in the $\binom{3\,1}{1\,3}$ structure. The benzene C-atom ring has a spacing of 2·20(5) to the metal surface with six identical Rh–C bond lengths of 2·30(5) Å. The corresponding $\binom{3\,1}{1\,3}$ distances are 2·25(5) and 2·35(5) Å. A possible Kekulé distortion is found, with $r \simeq 1{\cdot}51$ Å and $\beta \simeq 1{\cdot}3°$, which yields alternating C–C bond lengths of 1·46(15) and 1·58(15) Å in the (3×3) structure. The corresponding $\binom{3\,1}{1\,3}$ values are $r \simeq 1{\cdot}72$ Å, $\beta \simeq 4{\cdot}5°$ and C–C bond lengths of 1·33(15) and 1·81(15) Å. In both cases, the short C–C bonds lie above single metal atoms, while the long C–C bonds form bridges linking pairs of metal atoms.

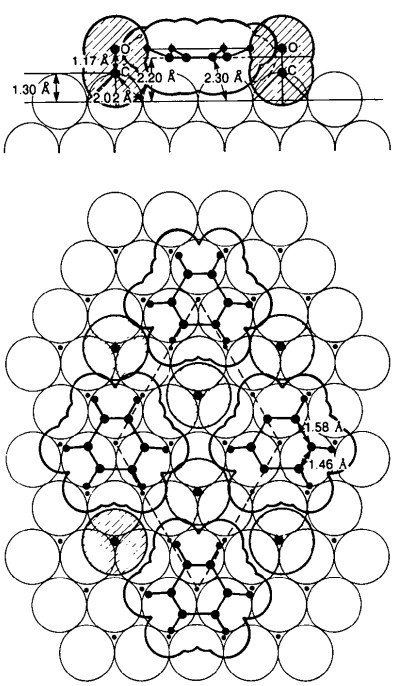

Fig. 4. Optimal structure for Rh(111)-(3×3)-C_6H_6+2CO, in side view at top and plan view at bottom. Van der Waals shapes are used. The CO molecules are shaded. The H-atom positions are guessed.

The optimal metal-carbon spacing for CO in the (3×3) structure is 1·30(10) Å, giving an Rh–C bond length of 2·02(7) Å, with a best C–O bond length of 1·17(10) Å. In the $\binom{31}{13}$ structure, we had found corresponding values of 1·50(5), 2·16(4) and 1·21(5) Å, respectively. The values of our error bars are based on various considerations: past experience with the uncertainties in the non-structural parameters and with the effects of the data-base size, as well as on the *R*-factor contour plots.

The best (3×3) structure has values of Zanazzi-Jona *R* factor, Pendry *R* factor and five-*R*-factor average of 0·24, 0·41 and 0·21, respectively. These can be compared with 0·40, 0·66 and 0·31, respectively, for $\binom{31}{13}$ and 0·42, 0·54 and 0·28, respectively, for Pt(111)-$(2\sqrt{3}\times4)$rect-$2C_6H_6+4CO$. In both cases on Rh(111) the muffin-tin zero level is found at 8(1) eV below the vacuum zero energy.

4. Discussion

Fig. 5 shows our best structure for Rh(111)-$\binom{31}{13}$-C_6H_6+CO (Van Hove, Lin & Somorjai, 1986). Fig. 6 shows the approximate structure of Rh(111)-$(2\sqrt{3}\times3)$rect-$2C_6H_6$, in which glide-plane symmetry imposes the choice of bridge site. For this CO-free structure a LEED intensity analysis has not been carried out to investigate the C_6 ring shape and other parameters. For further comparison, the structure found (Ogletree, Van Hove & Somorjai, 1987) for Pt(111)-$(2\sqrt{3}\times4)$rect-$2C_6H_6+4CO$ is shown in Fig. 7.

Table 2 compares the present structural result with the two other results for benzene on Rh(111) and Pt(111) surfaces, as well as with gas-phase benzene, benzene in organometallic complexes, acetylene and ethylene parallel bonded on Pt(111) and ethylidyne (CCH_3) bonded on Rh and Pt(111). Also, some theoretical results obtained with the extended Hückel molecular-orbital method are included for benzene on Rh(111). Table 3 makes similar comparisons for the structure of CO on various metal surfaces.

Van Hove, Lin & Somorjai (1986) contains a detailed discussion of a number of points arising out of such comparisons. We shall here summarize those points and focus on new aspects due to the present

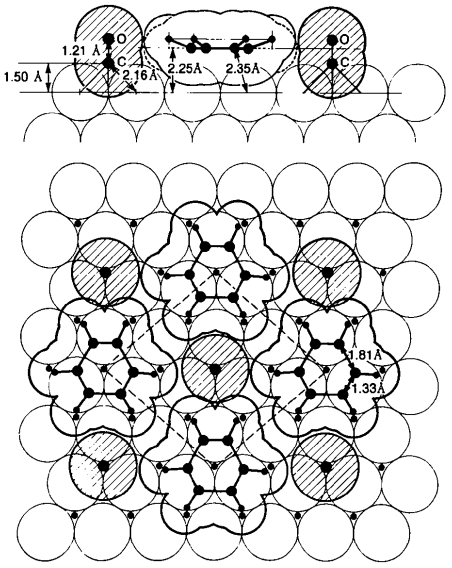

Fig. 5. As Fig. 4 for Rh(111)-c$(2\sqrt{3}\times4)$rect-C_6H_6+CO, from Van Hove, Lin & Somorjai (1986).

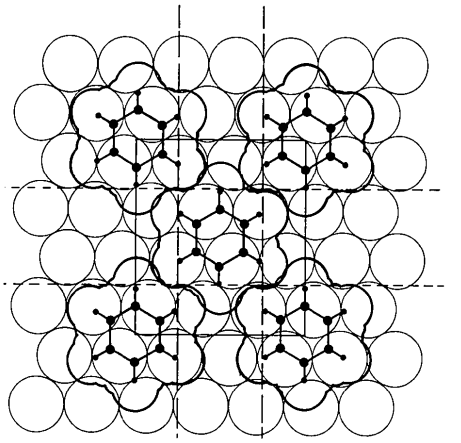

Fig. 6. As Figs. 4 and 5 for Rh(111)-$(2\sqrt{3}\times3)$rect-$2C_6H_6$, from Mate & Somorjai (1985). Dashed lines indicate glide planes perpendicular to the surface; the short dashed ones do not apply to the deeper metal layers.

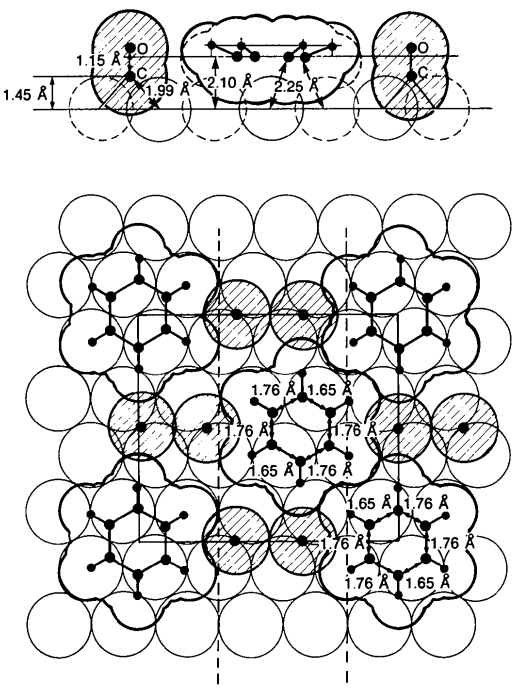

Fig. 7. As Figs. 4 and 6 for Pt(111)-$(2\sqrt{3}\times4)$rect-$2C_6H_6+4CO$, from Ogletree, Van Hove & Somorjai (1987).

Table 2. *Adsorption geometries of benzene*

System	$d^{<}_{C-C}$ (Å)	$d^{>}_{C-C}$ (Å)	$d_{\perp M-C}$ (Å)	d_{M-C} (Å)	Site
Rh(111)-c(2√3×4)rect-C_6H_6+CO[a]	1·33 (15)	1·81 (15)	2·25 (5)	2·35 (5)	Hollow
Rh(111)-(3×3)-C_6H_6+2CO[b]	1·46 (15)	1·58 (15)	2·20 (5)	2·30 (5)	Hollow
Rh(111)-(3×3)-C_6H_6 (theory)[c]	1·50	1·64	2·1	2·15	Hollow
Pt(111)-(2√3×4)rect-2C_6H_6+4CO[d]	1·65 (15)	1·76 (15)	2·10 (10)	2·25 (10)	Bridge
Pt(111)-C_6H_6 disordered[e]	1·39				
C_6H_6 on metal clusters[f]	1·39	1·48		2·27-2·32	Hollow
C_6H_6 molecule	1·397				
Pt(111)-(2×2)-C_2H_3 (ethylidyne)[g]	1·50 (10)		1·20 (1)	2·00 (7)	Hollow
Rh(111)-(2×2)-C_2H_3 (ethylidyne)[h]	1·45 (10)		1·31 (1)	2·03 (7)	Hollow
Pt(111)-C_2H_3(ethylidyne)[i]	1·49 (2)				
Pt(111)-C_2H_3 (ethylidyne)[j]	1·47 (3)				
C_2H_6 molecule	1·54				
Pt(111)-C_2H_4[k]	1·49 (3)				
C_2H_4 molecule	1·33				
Pt(111)-C_2H_2[k]	1·45 (3)				
C_2H_2 molecule	1·20				

References: (*a*) Van Hove, Lin & Somorjai (1986); (*b*) this work; (*c*) Garfunkel, Minot, Gavezzotti & Simonetta (1986); (*d*) Ogletree, Van Hove & Somorjai (1987); (*e*) Horsley, Stöhr, Hitchcock, Newbury, Johnson & Sette (1985); (*f*) Gomez-Sal, Johnson, Lewis, Raithby & Wright (1985); (*g*) Kesmodel, Dubois & Somorjai (1979); (*h*) Koestner, Van Hove & Somorjai (1982); (*i*) Wang, Slichter & Sinfelt (1985); (*j*) Horsley, Stöhr & Koestner (1985); (*k*) Stöhr, Sette & Johnson (1984).

Table 3. *Adsorption geometries of carbon monoxide*

System	$d_{\perp M-C}$ (Å)	d_{M-C} (Å)	D_{C-O} (Å)	Site
Pt(111)-c(4×2)-2CO[a]	1·85 (10)	1·85 (10)	1·15 (5)	Top
	1·55 (10)	2·08 (7)	1·15 (5)	Bridge
Rh(111)-(√3×√3)*R*30°-CO[b]	1·95 (10)	1·95 (10)	1·07 (10)	Top
Rh(111)-(2×2)-3CO[c]	1·87 (10)	1·94 (10)	1·15 (10)	Top
	1·52 (10)	1·52 (7)	1·15 (10)	Bridge
Ni(100)-c(2×2)-CO[d,e]	1·75 (10)	1·75 (10)	1·15 (10)	Top
Cu(100)-c(2×2)-CO[e]	1·90 (10)	1·90 (10)	1·13 (10)	Top
Pd(100)-(2√2×√2)*R*45°-2CO[f]	1·36 (10)	1·93 (7)	1·15 (10)	Bridge
Ru(0001)-(√3×√3)*R*30°-CO[g]	2·00 (7)	2·00 (7)	1·10 (10)	Top
Rh(111)-c(2√3×4)rect-CO+C_6H_6[h]	1·50 (5)	2·16 (4)	1·21 (5)	Hollow
Rh(111)-(3×3)-2CO+C_6H_6[i]	1·30 (10)	2·02 (7)	1·17 (10)	Hollow
Pt(111)-(2√3×4)rect-4CO+2C_6H_6[j]	1·45 (10)	1·99 (7)	1·15 (10)	Bridge
CO on metal clusters[k]		2·17-2·23	1·15-1·22	Hollow
CO on metal clusters[k]		2·00-2·09	1·07-1·18	Bridge
CO on metal clusters[k]		1·82-1·91	1·01-1·18	Top

References: (*a*) Ogletree, Van Hove & Somorjai (1986); (*b*) Koestner, Van Hove, Frost & Somorjai (1981); (*c*) Koestner, Van Hove & Somorjai (1982); (*d*) Tong, Maldonado, Li & Van Hove (1980); (*e*) Andersson & Pendry (1979); (*f*) Behm, Christmann, Ertl & Van Hove (1980); (*g*) Michalk, Moritz, Pfnür & Menzel (1983); (*h*) Van Hove, Lin & Somorjai (1986); (*i*) this work; (*j*) Ogletree, Van Hove & Somorjai (1986); (*k*) Chini, Longoni & Albano (1976).

availability of three distinct benzene surface structures. As discussed by Van Hove, Lin & Somorjai, (1986), the coadsorption of benzene and CO generates new ordering arrangements not present with the separate adsorption of benzene alone or CO alone. The adsorption sites themselves can be modified by coadsorption. The tendency is for benzene to move from bridge sites to hollow sites because of CO coadsorption on Rh(111) [the same h.c.p.-type hollow sites in both structures on Rh(111)]. The CO molecules tend towards higher coordination sites owing to coadsorption of benzene, especially on Rh(111). A charge transfer from benzene *via* the substrate to CO may explain this behavior. A C–O bond elongation, suggested particularly by the Rh(111)-$\binom{31}{13}$-C_6H_6+CO structure, is consistent with this picture. Less C–O elongation for Rh(111)-(3×3)-C_6H_6+2CO and Pt(111)-(2√3×4)rect-2C_6H_6+4CO might be explained by the sharing of benzene-donated charge among more CO molecules (this is also consistent with a slight increase of the C–O stretch frequency which occurs at the same time). It is not clear at this point why the Rh–C bond length for CO appears to differ considerably between the $\binom{31}{13}$ and the (3×3) structures: 2·16(4) and 2·02(7) Å, respectively.

The benzene adsorption site varies as is shown in Table 2. It may be added that, in the absence of CO, benzene is probably located in bridge sites both on Rh(111) (Van Hove, Lin & Somorjai, 1986) and on Pt(111) (Lin, Koestner, Van Hove & Somorjai, 1983). Our results indicate that the C_6 ring can distort in a way compatible with the site symmetry, *i.e.* with $C_{3v}(\sigma_d)$ symmetry over hollow sites and C_{2v} symmetry over bridge sites (or C_s symmetry if deeper metal layers are taken into account). The main effect of adsorption is a C_6 ring expansion, such that the mean ring radius is 1·58(15), 1·51(15) and 1·72(15) Å respectively, for Rh(111)-$\binom{31}{13}$-C_6H_6+CO, Rh(111)-(3×3)-C_6H_6+2CO and Pt(111)-(2√3×4)rect-2C_6H_6+4CO. In the $\binom{31}{13}$ structure we find also a strong variation between C–C bonds (three short

bonds and three long bonds), which is not as clearly apparent in the two other structures (we must keep in mind the relatively large error bars of ±0·15 Å on these distances). As mentioned in more detail by Van Hove, Lin & Somorjai (1986), similar but weaker distortions are found in organometallic complexes. New results (Gomez-Sal, Johnson, Lewis, Raithby & Wright, 1985) are now available for two complexes containing benzene symmetrically placed against a metal triangle, $Ru_6(CO)_{11}(C_6H_6)_2$ and $Os_3(CO)_9(C_6H_6)$. As Table 2 shows, these exhibit the Kekulé-type distortion of our $\binom{31}{13}$ structure. Although it is less strong, this distortion also features a C_6 ring expansion to a radius of 1·44(2) Å. Similar expansions are found with near-edge X-ray absorption fine structure (NEXAFS) measurements for acetylene and ethylene parallel bonded to the Pt(111) surface (Stöhr, Sette & Johnson, 1984). The extended-Hückel results (Garfunkel, Minot, Gavezzotti & Simonetta, 1986) also predict a ring expansion, to about 1·52 Å, and a possible Kekulé-type distortion with C–C bond lengths of up to 1·50 and 1·64 Å, for the short and long bonds. Ethylidyne (CCH_3) species have C–C bonds perpendicular to the surface. Although these bonds are not in direct contact with the metal, unlike the case of benzene, they provide a valuable reference point for comparison of C–C bond lengths: see Table 2.

Recent measurements with angle-resolved ultraviolet photoelectron spectroscopy have been made for benzene with and without CO on Rh(111) (Neumann, Mack, Bertel & Netzer, 1985). The case with CO had the (3×3) pattern, while the CO-free case is claimed to have the $\binom{31}{13}$ pattern (our results would suggest that this pattern is due to some coadsorbed CO). These data appear to indicate that no deviation from sixfold symmetry occurs, *i.e.* that all C–C bonds in the C_6 ring are equally long. Our results may well be consistent with these conclusions. In the (3×3) case, our Kekulé-type distortion is possibly slight while, in the CO-free case, our analogous result on Pt(111) also shows small variations between C–C bond lengths for bridge-site adsorption. It is also possible that photoemission is insensitive to small deviations from sixfold symmetry.

Finally, a connection can be suggested between our results and the catalytic reactivity of Rh and Pt for benzene reactions. The Pt(111) crystal face is an excellent catalyst for the production of benzene from *n*-hexane or *n*-heptane (dehydrocyclization). This is an important reaction that is utilized in petroleum refining to produce high-octane gasoline. The Rh(111) crystal face, however, cannot carry out this catalytic reaction because of the rapid fragmentation of benzene on the metal surface (hydrogenolysis) under the reaction conditions. It would be tempting to correlate the surface structures that adsorbed benzene forms on these two transition metal surfaces to their catalytic behavior. Perhaps the large Kekulé distortion of the adsorbed aromatic molecule observed in one of our structures on rhodium is indicative of preferential C–C bond breaking to produce CH and C_2H fragments, which occurs as the temperature is increased (Koel, Crowell, Bent, Mate & Somorjai, 1986). Benzene chemisorbed on the Pt(111) crystal face is less systematically distorted, exhibiting only a more uniform expansion of the ring. Perhaps such a structure is indicative of a benzene intermediate on the metal surface that can desorb intact at the higher temperatures and pressures of the catalytic reaction. Future studies will test further the possible correlation between molecular surface structures and catalytic reaction intermediates.

We thank C. Minot, M. Simonetta, A. Gavezzotti and E. Garfunkel for fruitful discussions, made possible by a NATO US–France exchange grant and a NSF US–Italy exchange grant. This work was supported by the Director, Office of Energy Research, Office of Basic Energy Sciences, Materials Science Division, of the US Department of Energy under Contract No. DE-AC03-76SF00098. Supercomputer time was also provided by the Office of Energy Research of the Department of Energy.

References

ANDERSSON, S. & PENDRY, J. B. (1979). *Phys. Rev. Lett.* **43**, 363-366.

BEHM, R. J., CHRISTMANN, K., ERTL, G. & VAN HOVE, M. A. (1980). *J. Chem. Phys.* **73**, 2984-2995.

CHINI, P., LONGONI, G. & ALBANO, V. G. (1976). *Adv. Organomet. Chem.* **14**, 285-344.

GARFUNKEL, E. L., MINOT, C., GAVEZZOTTI, A. & SIMONETTA, M. (1986). *Surf. Sci.* **167**, 177-197.

GLAND, J. L. & SOMORJAI, G. A. (1973). *Surf. Sci.* **38**, 157-186.

GOMEZ-SAL, M. P., JOHNSON, B. F. G., LEWIS, T., RAITHBY, P. R. & WRIGHT, A. H. (1985). *J. Chem. Soc. Chem. Commun.* pp. 1682-1684.

HORSLEY, J. A., STÖHR, J., HITCHCOCK, A. P., NEWBURY, D. C., JOHNSON, A. L. & SETTE, F. (1985). *J. Chem. Phys.* **83**, 6099-6170.

HORSLEY, J. A., STÖHR, J. & KOESTNER, R. J. (1985). *J. Chem. Phys.* **83**, 3146-3153.

KESMODEL, L. L., DUBOIS, L. H. & SOMORJAI, G. A. (1979) *J. Chem. Phys.* **70**, 2180-3153.

KOEL, B. E., CROWELL, J. E., BENT, B. E., MATE, C. M. & SOMORJAI, G. A. (1986). *J. Phys. Chem.* **90**, 2949-2956.

KOEL, B. E., CROWELL, J. E., MATE, C. M. & SOMORJAI, G. A. (1984). *J. Phys. Chem.* **88**, 1988-1996.

KOESTNER, R. J., VAN HOVE, M. A., FROST, J. C. & SOMORJAI, G. A. (1981). *Surf. Sci.* **107**, 439-458.

KOESTNER, R. J., VAN HOVE, M. A. & SOMORJAI, G. A. (1982). *Surf. Sci.* **121**, 321-336.

LIN, R. F., KOESTNER, R. J., VAN HOVE, M. A. & SOMORJAI, G. A. (1983). *Surf. Sci.* **134**, 161-183.

MASSARDIER, J., TARDY, B., ABON, M. & BERTOLINI, J. C. (1983). *Surf. Sci.* **126**, 154-162.

MATE, C. M. & SOMORJAI, G. A. (1985). *Surf. Sci.* **160**, 542-560.

MICHALK, G., MORITZ, W., PFNÜR, H. & MENZEL, D. (1983). *Surf. Sci.* **129**, 92-106.

NEUMANN, M., MACK, J. U., BERTEL, E. & NETZER, F. P. (1985). *Surf. Sci.* **155**, 629-638.
NYBERG, G. L. & RICHARDSON, N. V. (1979). *Surf. Sci.* **85**, 335-352.
OGLETREE, D. F., KATZ, J. E. & SOMORJAI, G. A. (1986). *Rev. Sci. Instrum.* **57**, 3012-3018.
OGLETREE, D. F., VAN HOVE, M. A. & SOMORJAI, G. A. (1986). *Surf. Sci.* **173**, 351-365.
OGLETREE, D. F., VAN HOVE, M. A. & SOMORJAI, G. A. (1987). In preparation.
STÖHR, J., SETTE, F. & JOHNSON, A. L. (1984). *Phys. Rev. Lett.* **53**, 1684-1687.
SURMAN, M., BARE, S. R., HOFMANN, P. & KING, D. A. (1983). *Surf. Sci.* **126**, 349-358.
TONG, S. Y., MALDONADO, A., LI, C. H. & VAN HOVE, M. A. (1980). *Surf. Sci.* **94**, 73-88.
TSAI, M. C. & MUETTERTIES, E. L. (1982). *J. Phys. Chem.* **86**, 5067-5071.
VAN HOVE, M. A., LIN, R. F. & SOMORJAI, G. A. (1983). *Phys. Rev. Lett.* **51**, 778-781.
VAN HOVE, M. A., LIN, R. F. & SOMORJAI, G. A. (1986). *J. Am. Chem. Soc.* **108**, 2532-2537.
WANG, P. K., SLICHTER, C. P. & SINFELT, J. H. (1985). *J. Phys. Chem.* **89**, 3606-3609.

Acta Cryst. (1987). B**43**, 376-382

Symmetry of Belladonna Mottle Virus: Rotation Function Studies

BY SANJEEV K. MUNSHI, CHAITANYA N. HIREMATH AND MATHUR R. N. MURTHY

Molecular Biophysics Unit, Indian Institute of Science, Bangalore 560 012, *India*

AND H. S. SAVITHRI

Department of Biochemistry, Indian Institute of Science, Bangalore 560 012, *India*

(*Received* 22 *July* 1986; *accepted* 10 *February* 1987)

Abstract

Belladonna mottle virus, a spherical plant virus belonging to the tymovirus group, was crystallized by precipitation with polyethylene glycol 6000 in sodium citrate buffer (pH 5·6). The crystals belong to rhombohedral space group $R3$ ($a \simeq 300$ Å, $\alpha \simeq 60°$) with one molecule in the unit cell, and diffract X-rays to 3·5 Å resolution. Owing to the special interaxial angle of ~60°, the lattice can also be described in terms of a pseudo-face-centred cubic cell. The face-centring vectors of the pseudo cell form the cell edges of the rhombohedral cell. The three-dimensional X-ray diffraction data on these crystals were collected using screenless oscillation photography to a resolution of 6 Å. 37 842 independent reflections with $I/\sigma(I) \geq 2·0$ were measured on 51 film pairs. The cell parameters were refined to $a = 295·4$ Å and $\alpha = 59·86°$ by a post-refinement procedure. A rotation function was calculated using data between 11 and 13 Å resolution. The function unambiguously reveals the particle icosahedral symmetry and orientation in the unit cell. The body diagonals of the pseudo-cubic cell are nearly tetrahedral. The icosahedral particle also has a set of tetrahedrally related threefold axes. The particle orientation is such that these two sets can be made coincident by a rotation of ~180° about the rhombohedral [111] direction.

Introduction

Belladonna mottle virus (BDMV) is a spherical plant virus consisting of a single-stranded, positive-sense RNA genome. Some of the biophysical properties of BDMV and its crystallization have been reported (Virudachalam, Heuss, Argos & Markley, 1983; Heuss, Mohana Rao & Argos, 1981). The related turnip-yellow mosaic virus (TYMV) has been extensively studied with respect to its biophysical and biochemical properties (Nixon & Gibbs, 1960; Klug, Longley & Leberman, 1966; Kaper, 1975; Jacrot, Chauvin & Witz, 1977; Katouzian-Safadi & Haenni, 1986). These studies reveal that the particles of TYMV are stabilized predominantly by the hydrophobic association of protein subunits (Kaper, 1975). Low-angle neturon scattering studies indicate that there is little, if any, penetration of the nucleic acid into the tightly packed protein coat (Jacrot *et al.*, 1977). In electron micrographs, TYMV appears to be constructed of 32 morphological units (Finch & Klug, 1966) consistent with $T = 3$ icosahedral symmetry (Caspar & Klug, 1962). In this paper we report crystallization of BDMV, collection and processing of X-ray diffraction data, and rotation function studies. The studies reveal the icosahedral symmetry of the virus particle and its orientation in the unit cell.

0108-7681/87/040376-07$01.50